Improved anti-inflammatory properties of xanthan gum hydrogel physically and chemically modified with yeast derived peptide

IOP Publishing Biomed. Mater. 18 (2023) 025026 https://doi.org/10.1088/1748-605X/acbd08

Biomedical Materials

PAPER

RECEIVED
6 December 2022

REVISED
19 January 2023

ACCEPTED FOR PUBLICATION
17 February 2023

PUBLISHED
3 March 2023

Improved anti-inflammatory properties of xanthan gum hydrogel physically and chemically modified with yeast derived peptide

Alex C Alavarse[1], Mahta Mirzaei[2,3,4], Amin Shavandi[2,*] and Denise F S Petri[1,*]

[1] Fundamental Chemistry Department, Institute of Chemistry, University of São Paulo, Av. Prof. Lineu Prestes 748, 05508-000 São Paulo, Brazil
[2] Université Libre de Bruxelles (ULB), École polytechnique de Bruxelles, 3BIO-BioMatter, Avenue F.D. Roosevelt, 50—CP 165/61, 1050 Brussels, Belgium
[3] Department of Environmental Technology, Food Technology and Molecular Biotechnology, Ghent University Global Campus, Incheon, Republic of Korea
[4] Department of Food Technology, Safety and Health, Faculty of Bioscience Engineering, Ghent University, Coupure Links 653, 9000 Ghent, Belgium
[*] Authors to whom any correspondence should be addressed.

E-mail: amin.shavandi@ulb.be and dfsp@iq.usp.br

Keywords: yeast peptides, xanthan gum, macrophages, anti-inflammation

Abstract

Bioactive peptides from natural resources with associated beneficial biological properties such as skin wound healing have drawn much attention. Polysaccharides with their biocompatibility, biodegradability, and ease of modification are suitable carriers for peptides delivery to the wound. In this study, a polysaccharide-peptide system was designed for potential wound healing applications. Xanthan hydrogels were modified with the yeast-derived peptide VW-9 with known biological properties via chemical conjugation using carbodiimide chemistry (XG-g-VW-9) or physically incorporation (XG-p-VW-9). Grafting VW-9 to the hydrogels increased the hydrogels' swelling degree and the release of the peptide from the hydrogels followed the Higuchi model indicating the peptide diffusion from the hydrogel matrix without hydrogel matrix dissolution. Both hydrogels were cytocompatible toward the tested fibroblast and macrophage cells. XG-p-VW-9 and XG-g-VW-9 reduce the level of tumor necrosis factor-alpha and interleukin-6 in cells activated with lipopolysaccharide more efficiently than free VW-9. Thus, VW-9-modified xanthan hydrogels may have the potential to be considered for skin wound healing.

1. Introduction

Inflammation is a biological response of the immune system that can be triggered by physical (burn, physical injury, foreign bodies, trauma, etc), chemical (glucose, fatty acids, toxins, alcohol, fluoride, nickel, etc) and biological (damaged cells) or infectious (bacteria, viruses) factors [1] Inflammatory processes stimulate cells to produce pro-inflammatory cytokines such as interleukin-1β (IL-1β), IL-6, and tumor necrosis factor-alpha (TNF-α), which are related to pathological pain [2]. Therefore, one way to reduce inflammation and pain is by inhibiting the excessive production of cytokines [2]. Designing biomaterials to suppress the inflammatory process might be challenging because sometimes intrinsic biomaterial characteristics might induce an inflammatory response [3]. Polysaccharide based hydrogels are interesting systems to carry and deliver anti-inflammatory agents and drugs due to their biocompatibility, inherent functional groups that endow active sites for bioconjugation and the possibility to create injectable, implantable and topical hydrogels [4, 5]. For instance, agarose hydrogels delivered antisense nucleotides to prevent the secretion of cytokines [6], intra-articular injection of chitosan thermosensitive hydrogels delivered diclofenac sodium [7], and tyramine-modified gellan gum hydrogels delivered anti cytokine dendrimer nanoparticles with the aid of a cartilage-on-a-chip system [8].

There is a plethora of anti-inflammatory peptides (AIPs) from plants, animals, and microorganisms [9, 10]. However, peptides might undergo enzymatic degradation, resulting in low bioavailability [11]. Conjugating peptides to polymers is a strategy to

increase AIP stability and gain synergistic properties [12]. For instance, AIP grafted to hydrogels formed by cysteine-terminated and thioester-terminated 4-armed poly(ethylene glycol) protected islet cells against cytokines action [13]. Although the literature has many reports about polysaccharide-peptide conjugates for drug delivery [12], there is scarce information about the conjugation of AIP on polysaccharides for anti-inflammatory therapy.

Yeast cells produce bioactive peptides due to their proteolytic activity during fermentation processes [14]. Yeast derived peptide VW9 (VLSTSFPPW) showed antioxidant and anti-inflammatory activity as well as a stimulating effect on fibroblasts and macrophages [15], making it an interesting molecule for the functionalization of wound healing biomaterials [16]. Xanthan gum (XG) is a microbial polysaccharide; the backbone has cellobiose as the repeating unit and side-chains consisting of a trisaccharide composed of D-mannose (β-1,4), D-glucuronic acid (β-1,2) and D-mannose, which are attached to alternate glucose residues in the backbone by α-1,3 linkages [17]. Beyond their use as drug carrier [18, 19], XG hydrogels shows favorable conditions for cell adhesion and proliferation [20, 21]. In this work, XG hydrogels were used as VW9 carriers. VW9 molecules were either physically incorporated into the hydrogels or chemically attached to the hydrogels via carbodiimide chemistry; the biocompatibility and anti-inflammatory properties of VW9 in both systems were evaluated in comparison to free VW9 molecules.

2. Experimental

2.1. Materials

XG (Xantural®, CP Kelco, Brazil) with a degree of pyruvate of 0.39, degree of acetyl of 0.42, and M_v of 1.3×10^6 g mol^{-1} [21], citric acid (CA, LabSynth, Brazil) and sodium hypophosphite (SHP, LabSynth, Brazil), Morpholinoethanesulfonic acid sodium salt (MES, Sigma-Aldrich, Brazil), N′-ethylcarbodiimide hydrochloride (EDC, Sigma-Aldrich, Brazil) and N-hydroxysuccinimide (NHS, Sigma-Aldrich, Brazil) were used as received. Milli-Q® water was used in all experiments. The peptide VW9 has the amino acid sequence Val-Leu-Ser-Thr-Ser-Phe-Pro-Pro-Trp (MW: 1032.52 Da, theoretical pI 5.58) and purity greater than 95% (SynthBio Engineering, China). Peptides containing biotin were also produced (SynthBio Engineering, China) to aid in the characterization of peptides conjugated to XG after streptavidin labeling and imaging using fluorescence microscopy.

2.1.1. Synthesis of XG hydrogels and peptide grafting via carbodiimide reaction

Solutions of XG were prepared in MilliQ water at 30 g l^{-1} in the presence of CA (3 g l^{-1}) and SHP (1.5 g l^{-1}) as crosslinker and catalyst, respectively, under magnetic stirring at 24 ± 1 °C. The solutions were poured into Petri dishes (diameter of 50 mm), and frozen for 24 h in a standard freezer at −24 °C, followed by 8 h of freeze-drying under vacuum (0.2 mbar). After freeze-drying, the samples were removed from the molds and heated for 7 min at 165 °C to promote the crosslinking [22]. The crosslinking results from the esterification reaction between citric acid groups and XG hydroxyl groups (scheme 1(a)) catalyzed by HPS, with the release of water molecules [21, 23]. After cooling down to (23 ± 1) °C, the unreacted molecules were removed by rinsing the samples with MilliQ water until the rinsing water achieved conductivity of ∼5 μS cm^{-1}. The samples were coded as XGH.

The conjugation of VW9 to XGH was mediated by the reaction with carbodiimide [24]. Briefly, the reaction between XG carboxylic acid groups and EDC molecules, in the presence of NHS, yields stable O-acylisourea groups that can react with VW9 amino groups, resulting in amide bonds (scheme 1(b)). EDC (0.768 g l^{-1}) and NHS (0.287 g l^{-1}) solutions were prepared in MES buffer solution (4.103 mg l^{-1}, pH = 6.5) to guarantee a successful reaction [24]. First, 100 μl of EDC solution was added to the freeze-dried XGH samples, which were cut as discs of 19 mm diameter, then 100 μl of NHS solution was added. The XGH samples were completely soaked by EDC and NHS solutions. After 20 min, 200 μl of VW9 solution (1.0 g l^{-1}) was added and then kept 12 h at 37 °C in a oven. These samples were coded as XG-g-VW9. For comparison, VW9 was physically incorporated in the XGH. The procedure was exactly the same, but in the absence of EDC and NHS. The samples were coded as XG-p-VW9. In sequence, the samples were washed for 1 h in distilled water and dried in oven (37 °C) before further characterization and tests.

2.2. Characterization of XGH, XG-p-VW9 and XG-g-VW9

The morphology of freeze-dried XGH, XG-p-VW9 and XG-g-VW9 was evaluated using scanning electron microscopy (SEM, FEI Quanta 200) in environmental mode; the samples were coated with gold prior to the analyses. Fourier-transform infrared vibrational spectroscopy in the attenuated total reflectance mode with 4 cm^{-1} of resolution and 32 scans (FTIR-ATR, Perkin Elmer Frontier) and elemental analyses (CNH, Perkin Elmer—2400 series (ii)) were performed to identify and quantify the chemical composition of XGH, XG-p-VW9 and XG-g-VW9. Circular dichroism (CD) spectra of XG, VW9 solutions and their mixture, and of XGH and XG-g-VW9 hydrogels were measured in the range of 190 nm to 300 nm with 0.5 nm of resolution and 5 nm of step size (CD, Jasco 815). For the CD measurements, hydrogel samples

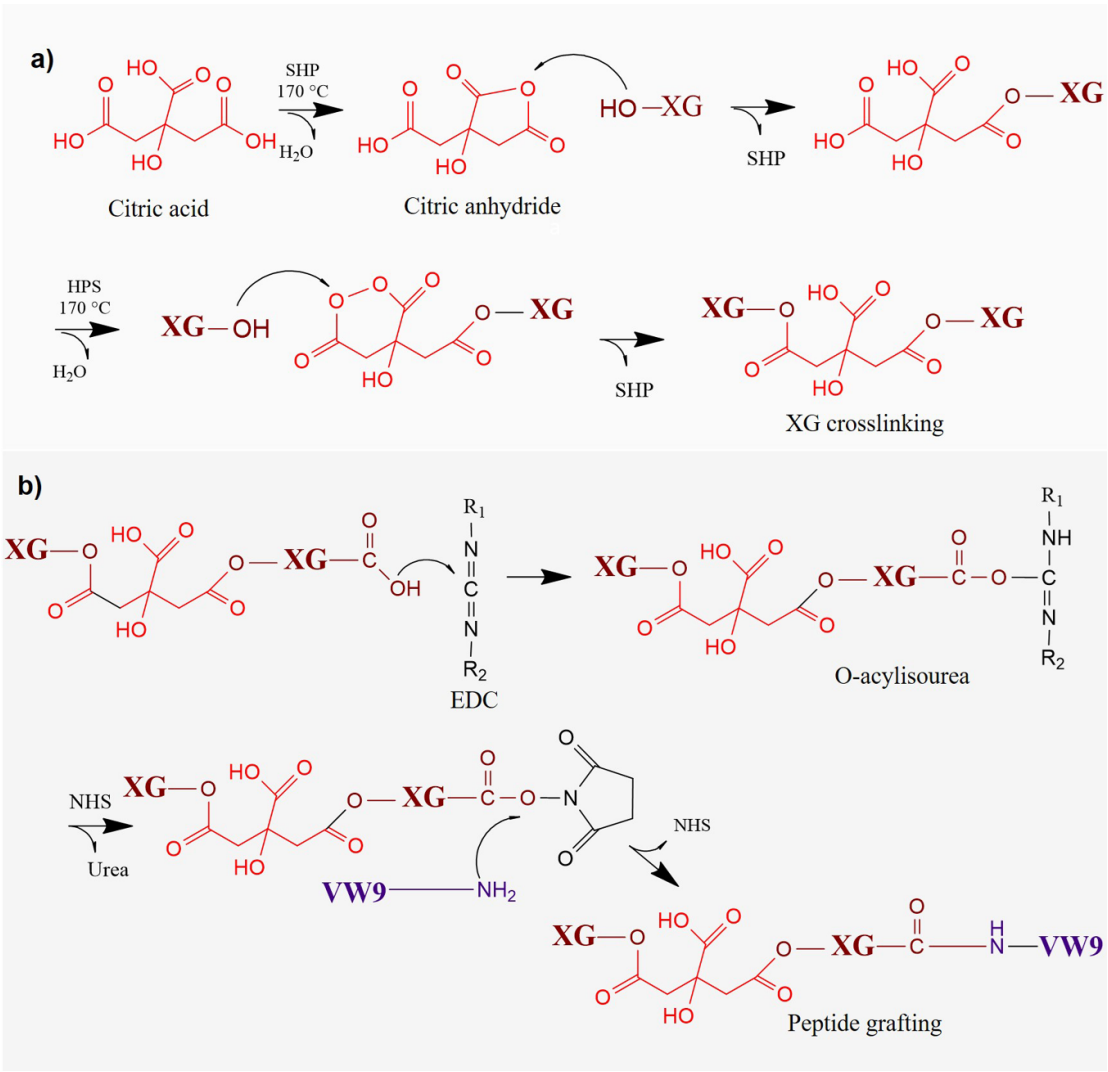

Scheme 1. (a) Crosslinking of XG chains with citric acid (b) and grafting of VW9 to XG chains mediated by EDC/NHS reaction.

were attached to the external cuvette wall and swollen with PBS solution (pH = 7.4). The swelling degree (SD) of XGH, XG-p-VW9 and XG-g-VW9 was gravimetrically determined from water sorption experiments at (24 ± 1) °C. For that, freeze-dried samples were weighed (precision 0.1 mg) to determine m_{dry}. Then, the samples were soaked in MilliQ water (pH 5.5) for 1 h, with the subsequent careful removal of surface water with tissue paper. The swollen hydrogels were then weighed to determine $m_{swollen}$. The SD was determined for triplicates by:

$$SD = \frac{m_{swollen} - m_{dry}}{m_{dry}}. \quad (1)$$

The chemically and physically binding of VW9 to XGH was assessed by fluorescence microscopy, using the specific biotin-streptavidin binding. A biotin modified VW9 variant ($VW9_{biotin}$) was either chemically grafted to XGH via EDC reaction or physically incorporated into XGH. The samples were fixed in paraformaldehyde 4% for 15 min at room temperature (RT), then washed in phosphate-buffered saline (PBS) and blocked for 30 min at RT in bovine serum albumin (BSA) 0.5% [25]. Streptavidin-Fluorescein isothiocyanate (FITC) (Sigma, USA) was used at 125 μg ml^{-1} and incubated for 1 h at RT. After washing, samples were disposed of in IBIDI μ-dish 35 mm imaging chambers and were observed on a confocal microscope (Zeiss LSM710) with a 10x/0.3 Plan NeoFluar or a 20x/0.8 Plan Apochromat objective. Images were analyzed using Fiji software [26] by segmenting the samples from the background using an intensity threshold and analyzing the mean intensity.

BCA protein assay kit (Merck, USA) was used to determine the release profile of the peptide from the hydrogels. Each hydrogel was immersed in PBS buffer (500 μl) and incubated at 37 °C for 48 h. Samples (20 μl) were taken and then replaced with new PBS buffer at time points up to 48 h. A microplate reader was used to determine the absorbance at 490 nm. The experimental data were fitted with

Korsmeyer–Peppas model (equation (2)) [27] and Higuchi model [28] (equation (3)):

$$\left(\frac{M_t}{M_{eq}}\right) = k_{KP} t^n \quad (2)$$

$$M_t = k_H \sqrt{t} \quad (3)$$

where M_t is the released amount at time 't', M_{eq} is the released amount at equilibrium, k_{KP} is a constant related to the release rate and 'n' is the diffusional coefficient. In the Higuchi model k_H is a constant related to the diffusion coefficient of the released molecule.

2.3. Biocompatibility of XGH, XG-p-VW9 and XG-g-VW9 with macrophages and fibroblasts

U937, a pro-monocytic human myeloid leukemia cell line (ATCC, CRL-1593.2), and fibroblasts (ATCC, CCL-186) were obtained from American Type Culture Collection. The cells were cultured in RPMI 1640 and Dulbecco's Modified Eagle Medium (DMEM) respectively, supplemented with 2 mM L-glutamine, 10% fetal bovine serum (FBS), and 100 unit ml^{-1} penicillin/streptomycin (Lonza Bioscience), according to ATCC guidelines. The U937 (passage number 12-16) and fibroblast cells (passage number 16-20) density were maintained at 100 000 viable cells ml^{-1}, respectively. Cells were incubated at 37 °C in a humidified atmosphere (5% CO_2). Cells were harvested once the cell confluency reached approximately 80%–90%. U937 was differentiated to macrophage-like cells (M0) after being treated with phorbol 12-myristate 13-acetate (PMA) (300 nm) for 24 h and then resting for another 24 h. To consider the compatibility of the prepared hydrogels with cells, they were soaked in culture media for about 3–4 h at 4 °C before cell culture. Macrophages and fibroblasts detached by trypsin and seeded on the surface of each hydrogel disk (100 K/1 ml/well). After 24 h, 48 h and 7 d of incubation at 37 °C, the viability of cells was evaluated. CellTiter 96 Aqueous one solution cell proliferation assay kit (Promega, USA) was used for this purpose, according to kit instruction. Additionally, the biocompatibility of the hydrogels was tested for Vero cells (ATCC, CCL-81), which were cultivated in flask cells T75 under DMEM high glucose medium and 10% of FBS. The *in vitro* cytotoxicity assays were performed using the solution extract, according to ISO 10993-5:2009 protocol [29], which involves the contact between cells seeded into the well plates with extract solution derived from the hydrogels. Metabolic activity was evaluated by the 3-(4,5-dimethyl-2-thiazolyl)−2,5-diphenyl-2H-tetrazolium bromide (MTT) assay. The cell viability of each sample was tested in quadruplicate ($n = 4$), dividing the absorbance reading corresponding to the sample by the absorbance reading of the control (only supplemented DMEM high medium).

The distribution of macrophages and fibroblasts on XGH, XG-p-VW9, XG-g-VW9 were investigated by fluorescent microscopy. Cells (200 000 cells/well) were seeded on the hydrogels. After 48 h, samples were retrieved from culture wells and gently washed with PBS and fixed in paraformaldehyde 4% for 15 min at RT, then washed in PBS and permeabilized by Triton X-100 0.2% for 5 min at RT. After blocking in 0.5% BSA for 30 min at RT, phalloidin-iFluor 488 (Abcam, ab176753, used at 1:1000 of stock solution) in blocking solution was added for 90 min at RT. Samples were washed and then scanned using a confocal microscope (Zeiss LSM710) with a 10x/0.3 Plan NeoFluar or a 20x/0.8 Plan Apochromat objective. The morphology of macrophage and fibroblast on XGH, XG-p-VW9, XG-g-VW9 was evaluated using SEM images. Samples were fixed in glutaraldehyde 2.5% in cacodylate buffer for at least 1 h, then post-fixed in osmium 2% in cacodylate buffer, washed and dehydrated in increasing concentrations of methanol (30%–50%–70%–95%–100% for 15 min each). Pure methanol was replaced by HMDS (hexamethyldisilazane) 100% which was left for drying under a chemical hood for a few days. Once samples were dried, they have been metallized with 20 nm of platinum before scanning using a FEI ESEM Quanta 200 using high vacuum and a 30 kV tension.

2.4. Anti-inflammatory activity of XGH, XG-p-VW9 and XG-g-VW9

Immunomodulatory activity of XGH, XG-p-VW9, XG-g-VW9 and free VW9, as control, was assessed by seeding macrophages at 200 000 cells in 1 ml per well in 24-well plates containing films and free peptide (0.5 mg ml^{-1}) for 22 h, followed by stimulation of cells with lipopolysaccharide (LPS) (*Escherichia coli* O55: B5, Sigma) (500 ng ml^{-1}) for 6 h. Supernatants were collected to determine IL-6 and TNF-α with specific ELISA kits according to the manufacturer's instruction (DuoSet ELISA Development System, Biotechne). Optical density was read immediately using a microplate reader at 450 nm and cytokine concentrations were evaluated using a standard curve.

3. Results and discussion

3.1. Characterization of XGH, XG-p-VW9 and XG-g-VW9

Figures 1(a)–(c) show typical SEM images of freeze-dried XGH, XG-p-VW9 and XG-g-VW9, respectively. All samples presented a similar porous structure, indicating that the physical incorporation of VW9 or the grafting of VW9 to the XG chains did not alter the porous structure. Figures 1(d)–(f) show the fluorescence microscopy along with the relative fluorescence intensity for XGH (negative control), XG-p-$VW9_{biotin}$ and XG-g-$VW9_{biotin}$, respectively.

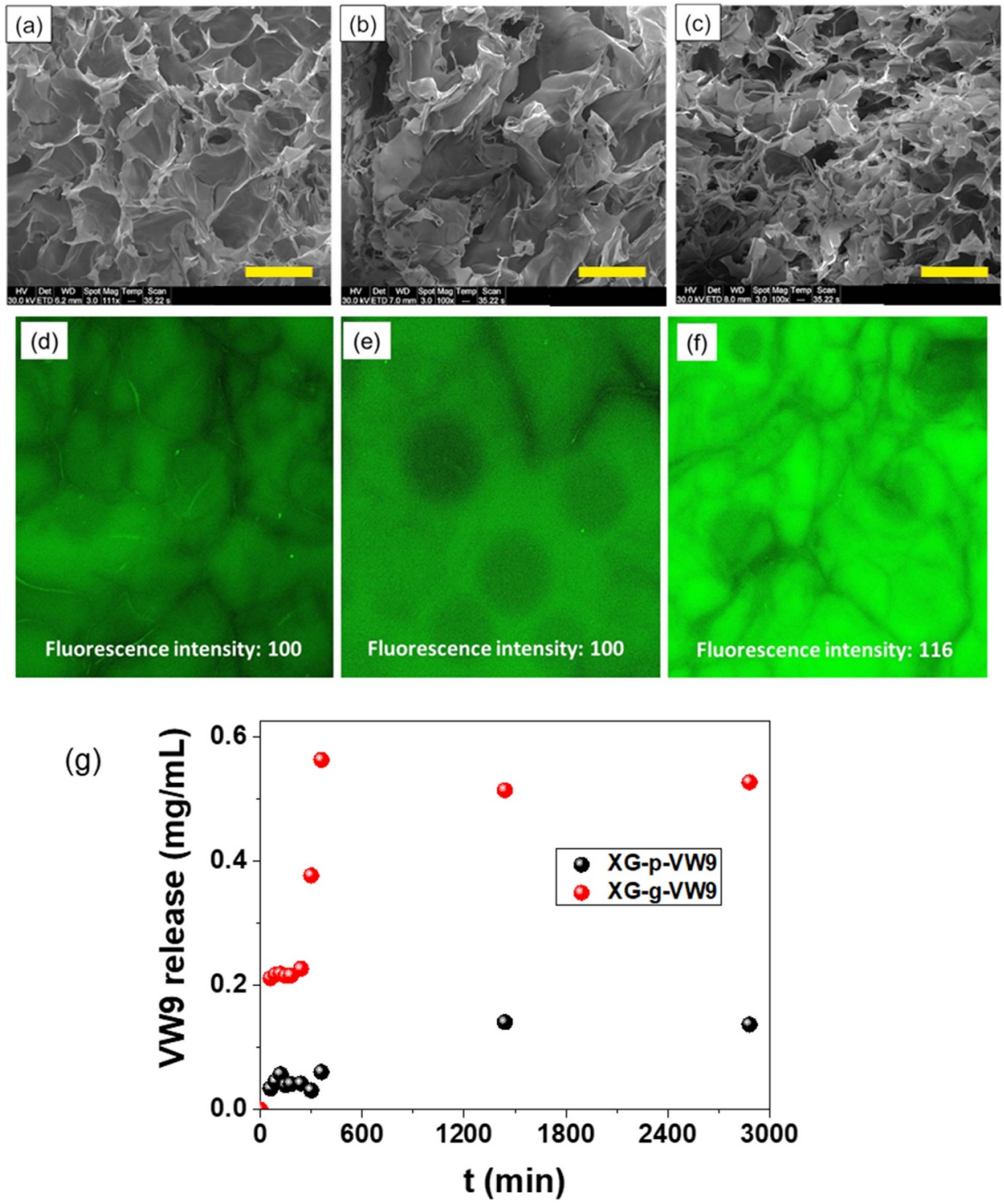

Figure 1. SEM images of (a) XGH, (b) XG-p-VW9 and (c) XG-g-VW9 freeze-dried samples (scale bar = 500 μm). Fluorescence microscopy images along with the relative intensities (λ_{em} = 525 nm) of (d) XGH, (e) XG-p-VW9 and (f) XG-g-VW9. (g) Release of VW9 from XG-p-VW9 and XG-g-VW9 samples measured by BCA protein assay.

There was a relative increase of fluorescence for XG-g-VW9$_{biotin}$ (figure 1(f)) samples due to the specific binding to streptavidin-FITC, indicating the successful grafting of the peptide to the hydrogel.

The fluorescence microscopy indicated that the physically incorporated peptide are leached from the hydrogels upon washing. To better understand the stability of VW9 in XG-p-VW9 and XG-g-VW9 samples, the release of VW9 was monitored as a function of time with the aid of BCA assay kit, XGH was used as the control sample. figure 1(g) shows that the cumulative release of VW9 from XG-p-VW9 increased up to 6 h, remaining approximately constant, and it was much more pronounced (∼fivefold) than the amount of VW9 released from XG-g-VW9. The fitting parameters (table 1) indicated that Higuchi model described better the release of VW9 from the hydrogels. Thus the release is controlled only by the diffusion of VW9 molecules without any significant effect on the matrix. The VW9 released from XG-g-VW9 presented a lower rate constant than that observed from XG-p-VW9. After the grafting reaction, a small amount of non-reacted VW9 might have remained bound to the grafted

Table 1. Fitting parameters were obtained for the release of VW9 from XG-p-VW9 and XG-g-VW9 hydrogels. k_{KP} (min^{-n}) and n stand for constant rate and diffusional coefficient (dimensionless) of Korsmeyer–Peppas model (equation (2)) k_H ($mg\ l^{-1}\ min^{-0.5}$) stands for Higuchi constant rate (equation (3)).

	Korsmeyer–Peppas			Higuchi	
Hydrogel	k_{KP} (min^{-n})	n	R^2	k_H ($mg\ ml^{-1}\ min^{-0.5}$)	R^2
XG-p-VW9	0.0371	0.4212	0.8636	0.013 78	0.8447
XG-g-VW9	0.1304	0.2602	0.7356	0.0030	0.9448

Table 2. Elemental analyses (CHN) and swelling degree (SD, g_{water}/g) determined for XGH, XG-p-VW9 and XG-g-VW9.

	C (%)	H (%)	N (%)	SD (g_{water}/g)
XG	34.9	5.9	0	19.0 ± 2.2
XG-p-VW9	34.7	5.9	0	21.1 ± 1.4
XG-g-VW9	34.1	6.1	1.0	25.4 ± 0.7
XG-EDC/NHS	34.8	6.0	0.7	—

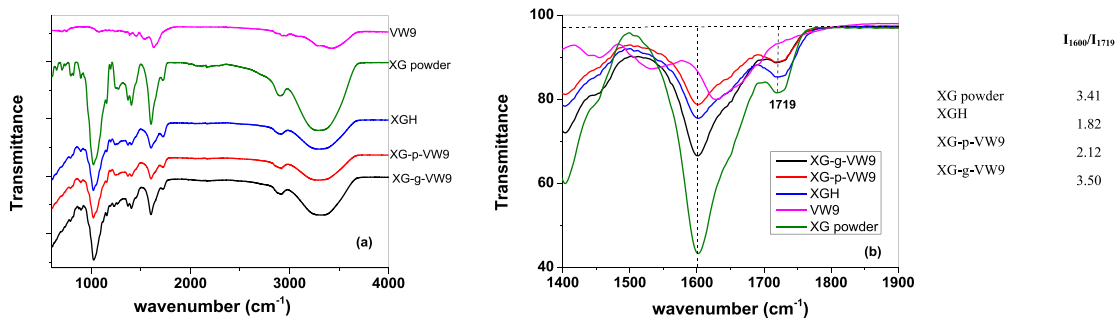

Figure 2. FTIR-ATR spectra of XG powder and hydrogels. (a) Spectral range from 600 cm^{-1} to 4000 cm^{-1}. (b) Spectral range from 1400 cm^{-1} to 1900 cm^{-1}, and the intensities I_{1600}/I_{1719} ratio.

VW9 due to van der Waals interactions and cooperativity. For XG-p-VW9 and XG-g-VW9 samples, the calculated M_{eq} (Korsmeyer–Peppas) values were 0.56 mg ml^{-1} and 0.14 mg ml^{-1}, respectively. The fitting curves to the Korsmeyer–Peppas and Higuchi models are provided as supplementary material SM1.

Table 2 shows the elemental analyses (C, H, N) for XGH, XG-p-VW9 and XG-g-VW9 samples after washing to remove the excess reactants and freeze-drying. XGH samples presented no nitrogen content, as expected. The XG-p-VW9 samples presented no content of N either, indicating that VW9 molecules were leached from the hydrogels during the washing process. The XG-g-VW9 samples presented 1.0% of N, but this content might stem from EDC molecules and VW9. To subtract the contribution of EDC to the N content, samples were prepared exactly like the XG-g-VW9, but without adding VW9. These samples, coded as XG-EDC, presented 0.70% N. Therefore, the grafting of VW9 contributed with 0.30% N to the total content of N in the XG-g-VW9 samples (1.00%). Since the N content in VW9 is 13.57%, 0.30% corresponds to 2.2% of VW9 grafted to XGH, i.e. each gram of XG-g-VW9 contains 0.022 g of VW9.

The SD values determined for XGH, XG-p-VW9 and XG-g-VW9 amounted to 19.0 ± 2.2 g_{water}/g, 21.1 ± 1.4 g_{water}/g and 25.4 ± 0.7 g_{water}/g, respectively (table 2); they are similar to SD value previously reported for xanthan hydrogels [23] and indicated that grafting VW9 to the hydrogels slightly increased their hydrophilicity.

Figure 2(a) shows the FTIR spectra obtained for XG (powder), VW9 (powder), XGH, XG-p-VW9 and XG-g-VW9. The spectra of XG powder, XGH, XG-p-VW9 and G-g-VW9 show the characteristic bands of polysaccharides in the 3500–3200 cm^{-1} region (O–H vibrational stretching); at 2930 cm^{-1} and 2850 cm^{-1} (symmetrical and asymmetrical C–H stretching); and in the 1240–850 cm^1 region (C–O and C–C stretching vibrations of the saccharide ring) [30]. Particularly important are the intensities ratio between carbonyl stretch (C=O) bands at 1600 cm^{-1} and 1719 cm^{-1}, which correspond to the acidic and ester forms, respectively, I_{1600}/I_{1719}. For XG powder, XGH and XGH-p-VW9 I_{1600}/I_{1719} values amounted to 3.4, 1.82 and 2.12 (figure 2(b)), respectively, indicating the increase of ester linkages after crosslinking [23, 24]. In the case of XG-g-VW9,

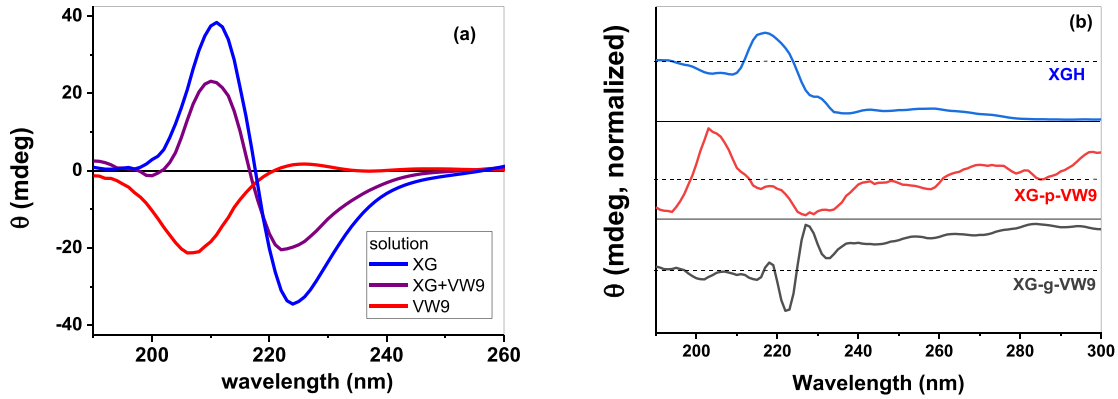

Figure 3. CD spectra were obtained for (a) XG at 6.6 g l^{-1}, VW9 at 0.5 g l^{-1} and the mixture of XG at 3.3 g l^{-1} and VW9 at 0.25 g l^{-1}, in aqueous solutions (pH 5.5). (b) XGH and XG-g-VW9 were swollen in PBS solution (pH = 7.4).

the ratio I_{1600}/I_{1719} of 3.50 might be attributed to the increase of I_{1600} due to the grafting of VW9. Pure VW9 presented the typical peptide bands in the 3500–3300 cm^{-1} region (N–H vibrational stretching), amide I at 1630 cm^{-1} and amide II at 1530 cm^{-1} [30]. Possibly, after grafting VW9 to XGH, the amide I band shifted to 1600 cm^{-1}, leading to the increase of I_{1600}/I_{1719} ratio.

Figure 3(a) shows the CD spectra of XG (6.6 g l^{-1}), VW9 (0.5 g l^{-1}) and their mixture (XG at 3.3 g l^{-1} and VW9 at 0.25 g l^{-1}) in aqueous solutions (pH 5.5). The CD spectra obtained for XG and XG/VW9 mixture presented similar features. The characteristic features of VW9 spectrum did not appear in the spectra obtained for the mixture probably due to the low concentration. The positive signal at ∼210 nm attributed to $n \rightarrow \pi^*$ transition of the carboxylate groups of XG (D-glucuronic acid and pyruvate groups) [18, 31] and the negative signal at ∼224 nm due to XG acetate groups [18] indicated the helix conformation of XG chains in the presence and absence of VW9. Pure VW9 presented a strong negative signal at ∼207 nm, typical of disordered structure, and a weak positive signal at ∼225 nm, indicating the presence of some helical structure [32]. Figure 3(b) shows the CD spectra for swollen XGH, XG-p-VW9 and XG-g-VW9 hydrogels. The XGH sample presented a positive signal at ∼217 nm, indicating that the helical conformation of XG chains was kept, even after crosslinking with citric acid. The CD spectra obtained for VW9 physically incorporated into the hydrogels resembled the spectra of their physical mixture in solution (figure 3(a)); the positive signal at ∼205 nm indicated that the helical conformation of XG chains and a broad negative signal in the range from 220 nm to 240 nm due to disordered coils. After chemical grafting VW9 to the XG chains (XG-g-VW9), the positive signal at ∼217 nm decreased considerably, but an intense positive signal at ∼227 nm appeared, indicating the presence of helical structures of XG chains. This shift to higher wavelength might be due to absorption flattening, which occurs when the absorbing species are not uniformly distributed in the sample [33]. Also, the interaction of XG chains with the grafted species which prevents the increase of joint points (entanglement), conform observed in rheology studies involving XG chains and proteins [34].

Noteworthy, the spectra obtained for XG-g-VW9 showed a weak positive band at 195 nm and a weak negative band at 201 nm, indicating β-sheet signature [35], which were not observed in the solution of free VW9 (figure 3(a)). The negative signals at ∼215 nm and ∼222 nm are typical of disordered structure.

3.2. Biocompatibility and anti-inflammatory properties of XGH, XG-p-VW9 and XG-g-VW9

Preliminarily, the biocompatibility of VW9 towards fibroblast and macrophage cells was investigated. Figure 4 shows that the addition of VW9 increased the cell viability compared to the control. For fibroblasts (figure 4(a)) VW9 at 0.5 mM presented the highest value of luminescence (∼2000 RLU) and at 0.25 mM and 1 mM (∼1800 RLU) the values were equivalent. For macrophages (figure 4(b)), the highest viability occurred at 0.25 mM of VW9 (8×10^6 RLU), whereas for 0.5 mM and 1 mM the values were equivalent ($\sim 5.8 \times 10^6$ RLU). Such values are at least twofold higher than the control value.

The viability of macrophage and fibroblast cells cultured on XGH, XG-p-VW9 and XG-g-VW9 after 24 h, 48 h and 7 d is presented in figures 4(c) and (d), respectively. At all phases of the experiment, the cell viability on XGH was higher than on XG-p-VW9 and XG-g-VW9, although the preliminary tests with pure VW9 showed excellent viability (figures 4(a) and (b)). After 7 d, the cell viability was reduced, and there was no significant difference in fibroblast's viability between samples. The inconsistency with the preliminary tests might be due to the fact that the cells were cultured directly on the hydrogels. The cells might have migrated to the interior of the hydrogels,

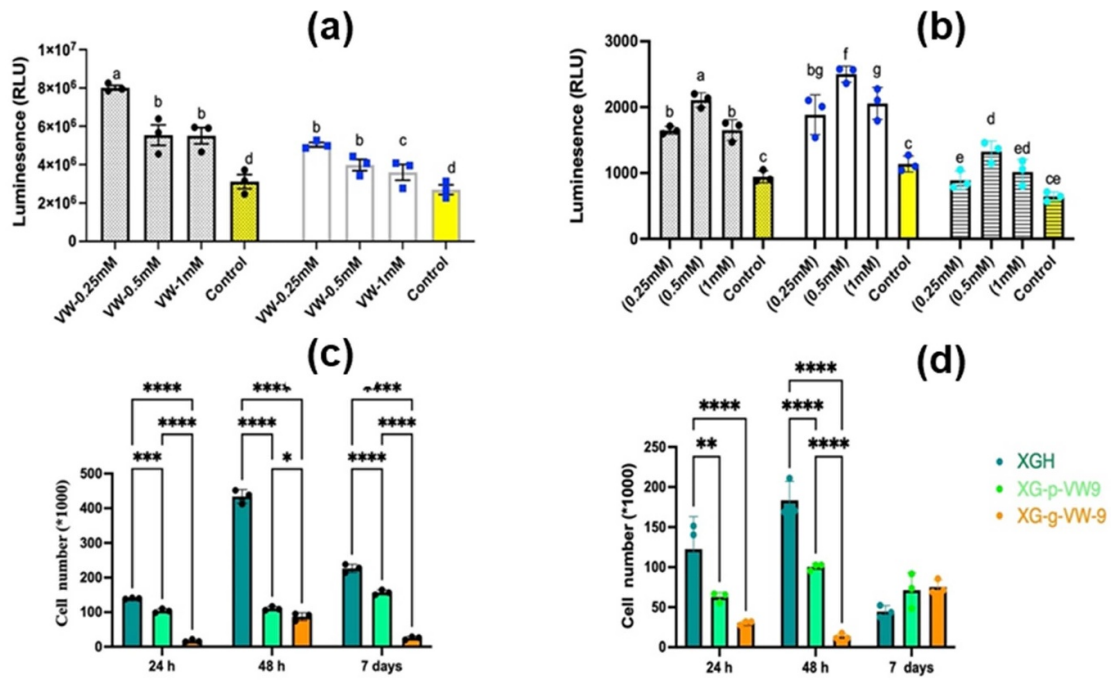

Figure 4. Biocompatibility of free VW9 (VW) incubated with macrophage (a) and fibroblast (b) cells for 24 h. Different letters present the significant differences between data ($P < 0.05$). The small dots are data points. The biocompatibility of XG hydrogels with (c) macrophage and (d) fibroblast cells. Results are presented as mean ± SD. * $P < 0.05$, ** $P < 0.01$, *** $P < 0.005$, and **** $P < 0.001$ represent the significant differences between data.

hindering their detection. To test this hypothesis, Vero cells were cultured with the extract solutions stemming from XGH and XG-g-VW9. The viability of Vero cells cultured with the extracts of XGH and XG-g-VW9 was similar or 2.4 times the viability in the control experiment (supplementary material SM2). These findings corroborate with those for pure VW9 (figures 4(a) and (b)) and support the hypothesis that the diffusion of cells to the interior of the hydrogels might have caused the low number of detected cells.

F-actin staining experiment by Phalloidin-iFluor 488 showed an even distribution of macrophages and fibroblasts on XGH, with a higher number of cells compared to XG-p-VW9 and XG-g-VW9 (figure 5). The population of fibroblasts was higher than macrophagè's population in all samples.

Macrophage and fibroblasts seeded on the XGH, XG-p-VW9 and XG-g-VW9 presented spherical morphology and dimensions of ∼10 μm, as shown in figures 6 and 7, respectively. These features corroborate with literature data. PMA-differentiated human macrophage-monocyte-like U937 cells presented spherical shapes with similar size [36, 37]. Fibroblasts seeded on tissue culture polystyrene [38], chitosan modified poly(caprolactone) [39] and xanthan/polypyrrole [40] scaffolds also presented spherical shape and dimensions of ∼10 μm.

The anti-inflammatory activity of VW-9 in free form was determined by comparing the levels of TNF-α and IL-6 in cells stimulated with LPS for 6 and 19 h and in cells pretreated with peptide (0.5 mg ml^{-1}) and stimulated with LPS. To investigate the anti-inflammatory effect of VW-9 physically (XG-p-VW-9) and chemically (XG-g-VW-9) attached to the hydrogels, The levels of TNF-α and IL-6 were compared in XGH sample as control and in XG-p-VW-9 and XG-g-VW-9, following LPS stimulation. Figure 8 shows that (i) the cytokine levels in XG-p-VW-9 and XG-g-VW-9 samples were lower than those in XGH, indicating the anti-inflammatory activity of VW-9 peptide-modified hydrogels, (ii)-a greater drop in TNF-α levels occurred in cells exposed to XG-p-VW9 and XG-g-VW-9 samples than in cells exposed to free VW-9 (figure 8(a)), (iii)-a greater drop in IL-6 levels occurred in cells exposed to XG-p-VW9 and XG-g-VW-9 samples than in cells exposed to free VW-9 (figure 8(b)), and (iv)-there was no significant difference in anti-inflammatory activity of XG-p-VW9 and XG-g-VW-9 samples. All together, our findings demonstrated that VW-9 exhibits anti-inflammatory activity in free form, as well as in physical and chemical graft forms. It could be because the anti-inflammatory activity of VW-9 is related to the interaction between peptide and receptors on the cell surface rather than the peptide's entry into the cell. More research is needed to confirm this theory. The diffusive process of VW-9 from XG-p-VW-9 and XG-g-VW-9 with constants of ∼0.013 78 and 0.0030 mg ml^{-1} min$^{-0.5}$, respectively (table 1), may explain why XG-p-VW-9 and XG-g-VW-9

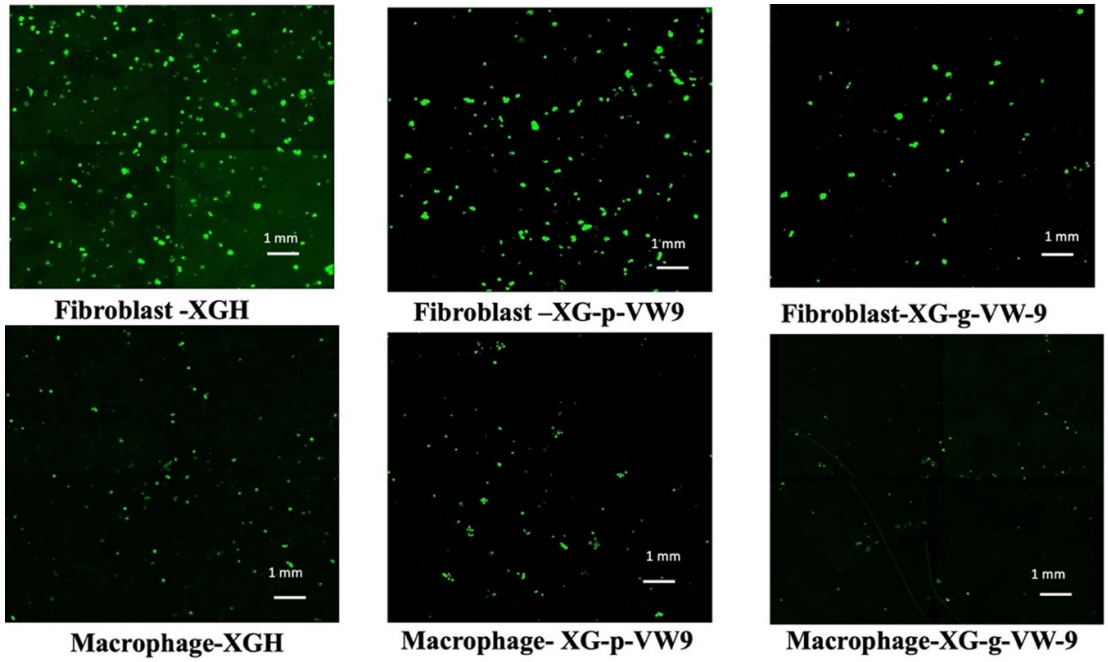

Figure 5. Confocal fluorescence microscopy image of fibroblasts and macrophages on XGH, XG-p-VW-9, and XG-g-VW-9 films. Phalloidin-iFluor 488 reagent binds to actin filaments (F-actin) and the iFluor dye is detected with Fluorescent microscope at Ex/Em = 493/517 nm.

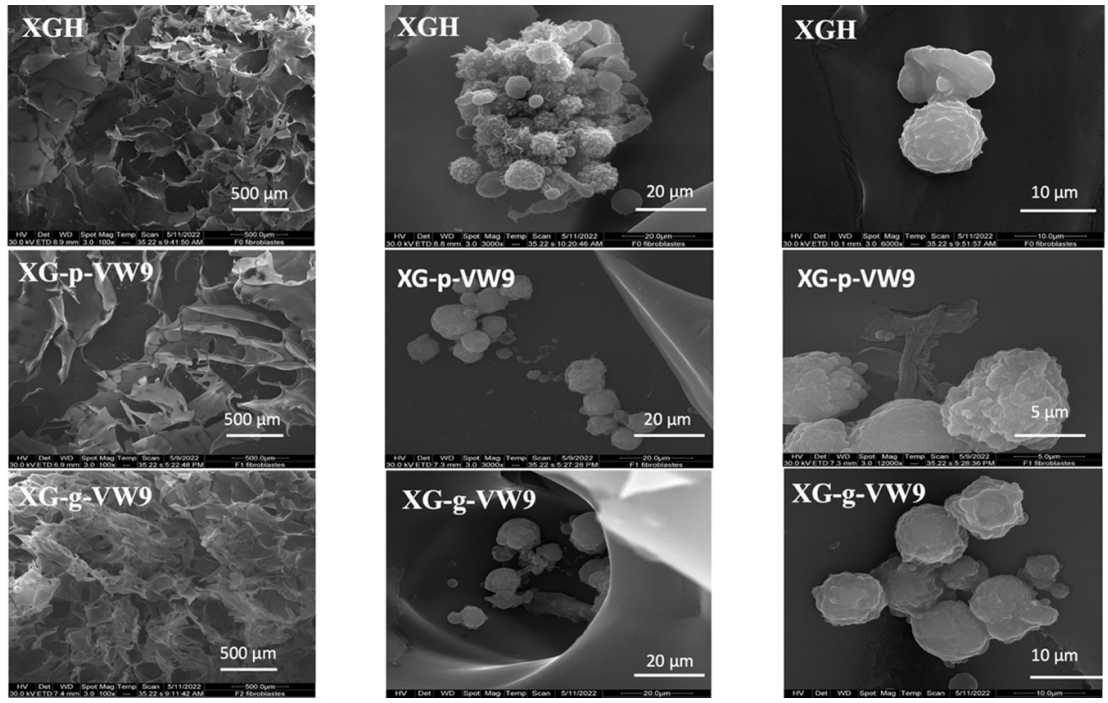

Figure 6. Scanning electron microscopy (SEM) images of macrophages on XGH, XG-p-VW9 and XG-g-VW9.

reduce the inflammatory response more efficiently than free form of VW-9. In physical grafting, the diffusion-controlled release kinetics is generally fast but conjugation via stronger interactions such as covalent bonds leads to a more sustained release [41]. The anti-inflammatory efficacy of grafted peptide, on the other hand, is regulated by the type of interface, the amino acids engaged in interaction, and the orientation of the peptide after grafting in covalent grafting of peptide in hydrogel [42]. Based

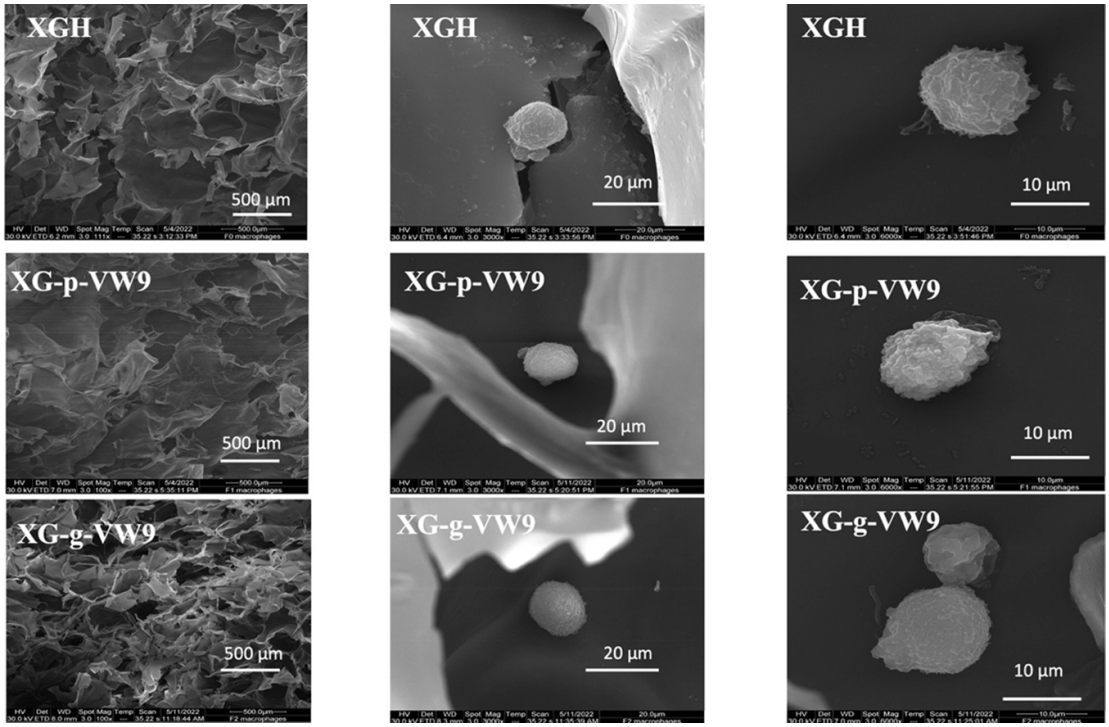

Figure 7. Scanning electron microscopy (SEM) images of fibroblasts on XGH, XG-p-VW9 and XG-g-VW9.

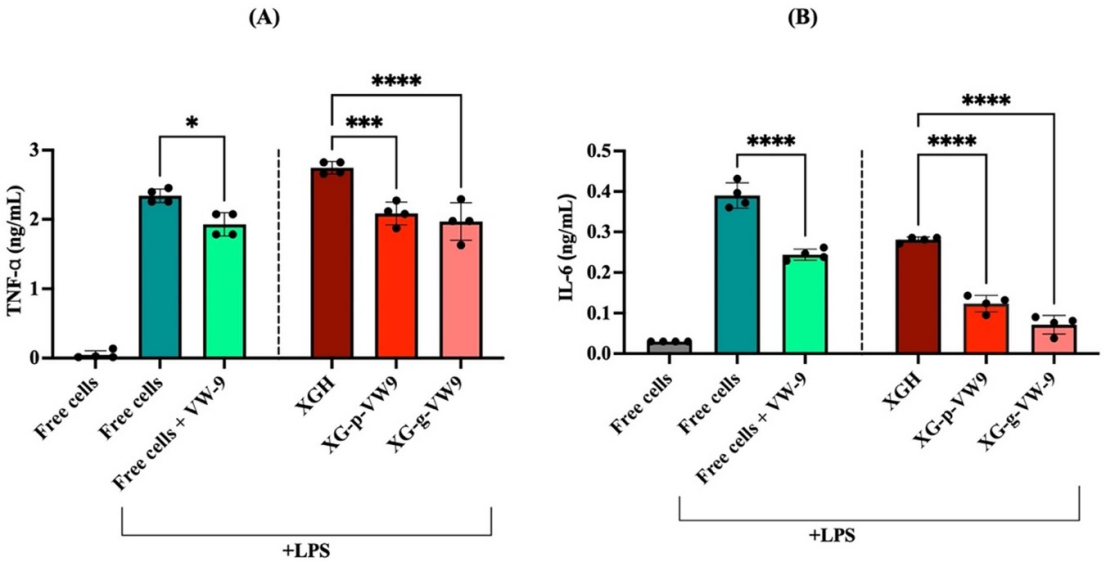

Figure 8. TNF-α (a) and IL-6 (b) levels in LPS-stimulated cells in free peptide and hydrogels. * $P < 0.05$, ** $P < 0.01$, *** $P < 0.005$, and **** $P < 0.001$ present the significant differences between data.

on that the C-terminal amino acid is the tryptophan (W), the activation of transcription factor NF-κB could be main mechanism which activates the anti-inflammatory function. This process was studied by Majumder *et al* with egg protein ovotransferrin derived peptides containing W as C-Terminal [34] .

Table 3 shows the maximal reduction of TNF-α and IL-6 levels secreted by LPS-stimulated cells in the presence of some polysaccharide-based anti-inflammatory systems reported in the recent literature, in comparison to the secretion of TNF-α and IL-6 by the cells in the absence of the anti-inflammatory agent. The data clearly show that the

Table 3. Maximal reduction of TNF-α and IL-6 cytokines values secreted by cells after incubation with carrier systems in comparison to the secretion of TNF-α and IL-6 cytokines in the absence of the anti-inflammatory agent.

System	Cell lineage	TNF-α (maximal reduction)	IL-6 (maximal reduction)	Reference
Chitosan-Ginsenoside compound on Au nanoparticles	Macrophages (RAW 264.7)	∼70%	∼50%	[43]
Chitosan hydrogels as carriers for acetylsalicylic acid (ASA) combined with cefuroxime (CFX), tetracycline (TCN) or amoxicillin (AMX)	Monocytes (THP-1)	ASA/CFX 64% ASA/TCN 67% ASA/AMX 87%	ASA/CFX 80% ASA/TCN 80% ASA/AMX 100%	[44]
Puerarin-loaded chitosan hydrogels	Macrophages (RAW 264.7)	60%	20%	[45]
Chitosan of different molecular weights	Macrophages (RAW 264.7)	156 kDa ∼ 19% 7.1 kDa ∼ 0%	156 kDa ∼ 50% 7.1 kDa ∼ 0%	[46]
Silymarin and curcumin loaded chitosan	Lung tissue	—	20%	[47]
3D graphene-based and *Gentiana straminea* polysaccharide	Macrophages (RAW 264.7)	∼27%	∼40%	[48]
Artemisinin, ellagic acid, epigallocatechin gallate, morusin incorporated to yeast glucan particles	Monocytes (THP-1-XBlue™-MD2-CD14)	∼50%	—	[49]
Levofloxacin loaded Chitosan/zeolite A	Human epithelia (NL20)	—	89.3%	[50]
XG-p-VW-9 XG-g-VW-9	Monocytes (U937)	∼10% ∼15%	∼70% ∼90%	This work

systems XG-p-VW-9 and XG-g-VW-9 have excellent performance, particularly, regarding the suppression of IL-6 secretion.

4. Conclusions

Although the wound healing process is complicated and dynamic and a single approach may not be ideal, the finding of the study indicates the potential of yeast-derived peptides for further evaluation toward wound healing. In this study, we designed a peptide-polysaccharide hydrogel system with potential anti-inflammatory properties using chemical conjugation and physical incorporation based on the yeast-derived peptide (VW-9) and xanthan. The analyzed data indicated the successful chemical grafting of the peptide while the peptide leached out of the hydrogel in case of physical incorporation. The peptide-modified hydrogels were shown to have anti-inflammatory activity and were not toxic to the tested cells and we may conclude that the diffusion of the peptide from the hydrogel systems and the peptide chemically bound to the hydrogels were more efficient in reducing the tested inflammatory markers compared to the free peptide. Nevertheless, further studies are required to reveal the exact mechanism of the observed anti-inflammatory and the involved pathways. In future studies, we will evaluate the cell encapsulation in the hydrogel systems to have a better understanding of the cell–matrix interactions.

Data availability statement

All data that support the findings of this study are included within the article (and any supplementary files).

Acknowledgments

This work was supported by Fundação de Amparo à Pesquisa do Estado de São Paulo FAPESP (Grant Nos. 2018/13492–2, 2019/22671-0 and 2020/01907-3). A S acknowledges financial support from FNRS-Fonds de la Recherche Scientifique for projets bilatéraux de mobilité (PINT-BILAT-M) R.M014.19 (35704283). M M acknowledges the fellowship provided by the European Program in IF@ULB-MARIE SKLODOWSKA-CURIE cofound action (European Horizon 2020).

Author contributions

Alex C Alavarse: Investigation, Methodology, Data curation, Writing- Original draft preparation **Mahta Mirzaei:** Investigation, Methodology, Data curation, Writing- Original draft preparation **Amin Shavandi:** Conceptualization, Project administration, Writing- Reviewing and Editing **Denise F S Petri:** Conceptualization, Project administration, Writing- Reviewing and Editing

ORCID iD

Amin Shavandi https://orcid.org/0000-0002-0188-3090

References

[1] Chen L *et al* 2017 Inflammatory responses and inflammation-associated diseases in organs *Oncotarget* **9** 7204–18
[2] Zhang J M and An J 2007 Cytokines, inflammation and pain *Int. Anesthesiol. Clin.* **45** 27
[3] Fenton O S, Olafson K N, Pillai P S, Mitchell M J and Langer R 2018 Advances in biomaterials for drug delivery *Adv. Mater.* **30** 1705328
[4] Jalalvandi E and Shavandi A 2018 In situ-forming and pH-responsive hydrogel based on chitosan for vaginal delivery of therapeutic agents *J. Mater. Sci: Mater. Med.* **29** 158
[5] Jalalvandi E and Shavandi A 2019 Shear thinning/self-healing hydrogel based on natural polymers with secondary photocrosslinking for biomedical applications *J. Mech. Behav. Biomed. Mater.* **90** 191–201
[6] Dong L, Xia S, Chen H, Chen J and Zhang J 2009 Spleen-specific suppression of TNF-α by cationic hydrogel-delivered antisense nucleotides for the prevention of arthritis in animal models *Biomaterials* **30** 4416–26
[7] Qi X, Qin X, Yang R, Qin J, Li W, Luan K, Wu Z and Song L 2016 Intra-articular administration of chitosan thermosensitive *in situ* hydrogels combined with diclofenac sodium–loaded alginate microspheres *J. Pharm. Sci.* **105** 122–30
[8] Oliveira I M, Carvalho M R, Fernandes D C, Abreu C M, Maia F R, Pereira H, Caballero D, Kundu S C, Reis R L and Oliveira J M 2021 Modulation of inflammation by anti-TNF α mAb-dendrimer nanoparticles loaded in tyramine-modified gellan gum hydrogels in a cartilage-on-a-chip model *J. Mater. Chem.* B **9** 4211–8
[9] Dadar M, Shahali Y, Chakraborty S, Prasad M, Tahoori F, Tiwari R and Dhama K 2018 Antiinflammatory peptides: current knowledge and promising prospects *Inflamm. Res.* **68** 125–45
[10] Jenab A, Roghanian R and Emtiazi G 2020 Bacterial natural compounds with anti-inflammatory and immunomodulatory properties *Drug Des. Devel. Ther.* **14** 3787–801
[11] Werle M and Bernkop-Schnürch A 2006 Strategies to improve plasma half life time of peptide and protein drugs *Amin. Acids* **30** 351–67
[12] Song H-Q, Fan Y, Hu Y, Cheng G, Xu F-J, Song H-Q, Xu F-J, Fan Y, Hu Y and Cheng G 2021 Polysaccharide–peptide conjugates: a versatile material platform for biomedical applications *Adv. Funct. Mater.* **31** 2005978
[13] Su J, Hu B H, Lowe W L, Kaufman D B and Messersmith P B 2010 Anti-inflammatory peptide-functionalized hydrogels for insulin-secreting cell encapsulation *Biomaterials* **31** 308–14
[14] Mirzaei M, Shavandi A, Mirdamadi S, Soleymanzadeh N, Motahari P, Mirdamadi N, Moser M, Subra G, Alimoradi H and Goriely S 2021 Bioactive peptides from yeast: a comparative review on production methods, bioactivity, structure-function relationship, and stability *Trends Food Sci. Technol.* **118** 297–315
[15] Mirdamadi S, Mirzaei M, Soleymanzadeh N, Safavi M, Bakhtiari N and Zandi M 2021 Antioxidant and cytoprotective effects of synthetic peptides identified from Kluyveromyces marxianus protein hydrolysate: insight into the molecular mechanism *Lwt* **148** 111792
[16] Mirzaei M, Shavandi A, Dodi G, Gardikiotis I, Pasca S-A, Mirdamadi S, Soleymanzadeh N, Alimoradi H, Moser M and Goriely S 2022 A yeast-derived peptide promotes skin wound healing by stimulating effects on fibroblast and immunomodulatory activities *SSRN Electron. J.* accepted (https://doi.org/10.2139/ssrn.4030328)
[17] Petri D F S 2015 Xanthan gum: a versatile biopolymer for biomedical and technological applications *J. Appl. Polym. Sci.* **132** 42035
[18] Bueno V B and Petri D F S 2014 Xanthan hydrogel films: molecular conformation, charge density and protein carriers *Carbohydr. Polym.* **101** 897–904
[19] Bueno P V A, Hilamatu K C P, Carmona-Ribeiro A M and Petri D F S 2018 Magnetically triggered release of amoxicillin from xanthan/Fe_3O_4/albumin patches *Int. J. Biol. Macromol.* **115** 792–800
[20] Glaser T, Bueno V B, Cornejo D R, Petri D F S and Ulrich H 2015 Neuronal adhesion, proliferation and differentiation of embryonic stem cells on hybrid scaffolds made of xanthan and magnetite nanoparticles *Biomed. Mater.* **10** 045002
[21] Alavarse A C, Frachini E C G, Silva J B, Dos S P R, Ulrich H and Petri D F S 2022 Amino acid decorated xanthan gum coatings: molecular arrangement and cell adhesion *Carbohydr. Polym. Technol. Appl.* **4** 100227
[22] Toledo P V O and Petri D F S 2019 Hydrophilic, hydrophobic, Janus and multilayer xanthan based cryogels *Int. J. Biol. Macromol.* **123** 1180–8
[23] Bueno V B, Bentini R, Catalani L H and Petri D F S 2013 Synthesis and swelling behavior of xanthan-based hydrogels *Carbohydr. Polym.* **92** 1091–9
[24] Alavarse A C, Frachini E C G, da Silva R L C G, Lima V H, Shavandi A and Petri D F S 2022 Crosslinkers for polysaccharides and proteins: synthesis conditions, mechanisms, and crosslinking efficiency, a review *Int. J. Biol. Macromol.* **202** 558–96
[25] Camacho P, Busari H, Seims K B, Schwarzenberg P, Dailey H L and Chow L W 2019 3D printing with peptide–polymer conjugates for single-step fabrication of spatially functionalized scaffolds *Biomater. Sci.* **7** 4237–47
[26] Schindelin J *et al* 2012 Fiji: an open-source platform for biological-image analysis *Nat. Methods* **9** 676–82
[27] Ritger P L and Peppas N A 1987 A simple equation for description of solute release II. Fickian and anomalous release from swellable devices *J. Control. Release* **5** 37–42

[28] Siepmann J and Peppas N A 2011 Higuchi equation: derivation, applications, use and misuse *Int. J. Pharm.* **418** 6–12
[29] International Organization for Standardization 2019 ISO 10993-5
[30] Silverstein R, MBassler G C and Morrill T 1991 Chapter three: infrared spectrometry *Spectrometric Identification of Organic Compounds* 5th edn, ed D Sawicki and J Stiefel (New York: Wiley) pp 91–164
[31] Eren N M, Santos P H S and Campanella O 2015 Mechanically modified xanthan gum: rheology and polydispersity aspects *Carbohydr. Polym.* **134** 475–84
[32] Bakshi K, Liyanage M R, Volkin D B and Middaugh C R 2014 Circular dichroism of peptides *Methods Mol. Biol.* **1088** 247–53
[33] Castiglioni E, Abbate S, Longhi G and Gangemi R 2007 Wavelength shifts in solid-state circular dichroism spectra: a possible explanation *Chirality* **19** 491–6
[34] Majumder K, Chakrabarti S, Davidge S T and Wu J 2013 Structure and activity study of egg protein ovotransferrin derived peptides (IRW and IQW) on endothelial inflammatory response and oxidative stress *J. Agric. Food Chem.* **61** 2120–9
[35] Li X, Li J, Gao Y and Kuang Y Shi J and Xu B 2010 Molecular nanofibers of olsalazine form supramolecular hydrogels for reductive release of an anti-inflammatory agent *J. Am. Chem. Soc.* **132** 17707–9
[36] Someya A, Moss J and Nagaoka I 2010 The guanine nucleotide exchange protein for ADP-ribosylation factor 6, ARF-GEP100/BRAG2, regulates phagocytosis of monocytic phagocytes in an ARF6-dependent process *J. Biol. Chem.* **285** 30698–707
[37] Cosío B G, Jahn A, Iglesias A and Shafiek H Busquets X and Agustí A 2015 Haemophilus influenzae induces steroid-resistant inflammatory responses in COPD *BMC Pulm. Med.* **15** 1–8
[38] Nguyen T-H and Lee B-T 2012 The effect of cross-linking on the microstructure, mechanical properties and biocompatibility of electrospun polycaprolactone–gelatin/PLGA–gelatin/PLGA–chitosan hybrid composite *Sci. Technol. Adv. Mater.* **13** 035002
[39] Mei N, Chen G, Zhou P, Chen X, Shao Z-Z, Pan L-F and Wu C-G 2005 Biocompatibility of poly(ε-caprolactone) scaffold modified by chitosan—the fibroblasts proliferation *in vitro J. Biomater. Appl.* **19** 323–39
[40] Bueno V B, Takahashi S H, Catalani L H, de Torresi S I C and Petri D F S 2015 Biocompatible xanthan/polypyrrole scaffolds for tissue engineering *Mater. Sci. Eng.* C **52** 121–8
[41] Barbosa M, Martins M C L and Gomes P 2015 Grafting techniques towards production of peptide-tethered hydrogels, a novel class of materials with biomedical interest *Gels* **1** 194–218
[42] Stevens J S, de Luca A C, Downes S, Terenghi G and Schroeder S L M 2014 Immobilisation of cell-binding peptides on poly-ε-caprolactone (PCL) films: a comparative XPS study of two chemical surface functionalisation methods *Surf. Interface Anal.* **46** 673–8
[43] Jie M X, Choi H S, Park H R and Kim Y J 2022 Structural characterization and anti-inflammatory properties of green synthesized chitosan/compound K-gold nanoparticles *Int. J. Biol. Macromol.* **213** 247–58
[44] Andrade Del Olmo J, Pérez-Álvarez L, Sáez-Martínez V, Benito-Cid S, Ruiz-Rubio L, Pérez-González R, Vilas-Vilela J L and Alonso J M 2022 Wound healing and antibacterial chitosan-genipin hydrogels with controlled drug delivery for synergistic anti-inflammatory activity *Int. J. Biol. Macromol.* **203** 679–94
[45] Yuan H, Li W, Song C and Huang R 2022 An injectable supramolecular nanofiber-reinforced chitosan hydrogel with antibacterial and anti-inflammatory properties as potential carriers for drug delivery *Int. J. Biol. Macromol.* **205** 563–73
[46] Chang S H, Lin Y Y, Wu G J, Huang C H and Tsai G J 2019 Effect of chitosan molecular weight on anti-inflammatory activity in the RAW 264.7 macrophage model *Int. J. Biol. Macromol.* **131** 167–75
[47] Hanafy N A N and El-Kemary M A 2022 Silymarin/curcumin loaded albumin nanoparticles coated by chitosan as muco-inhalable delivery system observing anti-inflammatory and anti COVID-19 characterizations in oleic acid triggered lung injury and *in vitro* COVID-19 experiment *Int. J. Biol. Macromol.* **198** 101–10
[48] Shi S, Wang G, Liu J, Liu S, Xu Q, Lan X, Feng J, Sun J, Zhang W and Wang J 2021 Gentiana straminea Maxim. polysaccharide decolored via high-throughput graphene-based column and its anti-inflammatory activity *Int. J. Biol. Macromol.* **193** 1727–33
[49] Šalamúnová P, Cupalová L, Majerská M, Treml J, Ruphuy G, Šmejkal K, Štěpánek F, Hanuš J and Hošek J 2021 Incorporating natural anti-inflammatory compounds into yeast glucan particles increases their bioactivity *in vitro Int. J. Biol. Macromol.* **169** 443–51
[50] Mostafa M, El-Meligy M A and Sharaf M Soliman A T and AbuKhadra M R 2021 Insight into chitosan/zeolite-a nanocomposite as an advanced carrier for levofloxacin and its anti-inflammatory properties; loading, release, and anti-inflammatory studies *Int. J. Biol. Macromol.* **179** 206–16